Important Notice to Authors

No further publication processing will occur until we receive your response to this proof.

Attached is a PDF proof of your forthcoming article in *Physical Review Letters*. The article accession code is LG17581.

Your paper will be in the following section of the journal: LETTERS — General Physics: Statistical and Quantum Mechanics, Quantum Information, etc.

Please note that as part of the production process, APS converts all articles, regardless of their original source, into standardized XML that in turn is used to create the PDF and online versions of the article as well as to populate third-party systems such as Portico, Crossref, and Web of Science. We share our authors' high expectations for the fidelity of the conversion into XML and for the accuracy and appearance of the final, formatted PDF. This process works exceptionally well for the vast majority of articles; however, please check carefully all key elements of your PDF proof, particularly any equations or tables.

Figures submitted electronically as separate files containing color appear in color in the online journal.
However, all figures will appear as grayscale images in the print journal unless the color figure charges have been paid in advance, in accordance with our policy for color in print (https://journals.aps.org/authors/color-figures-print).

Specific Questions and Comments to Address for This Paper

The numbered items below correspond to numbers in the margin of the proof pages pinpointing the source of the question and/or comment. The numbers will be removed from the margins prior to publication.

1 Note that PRL guidelines require italic font for single-letter acronyms and single-letter variables and abbreviations in text and in math. Roman font is reserved for single-letter chemical symbols such as O and H and single-letter units of measure such as “g (for gram) and “J (for joule). Your math terms have been adjusted accordingly. Please ensure that your meaning has not been changed.

2 Please review the confirmation funding information section of the proof’s cover letter and respond as appropriate. We must receive that the funding agencies have been properly identified before the article can publish.

3 The references have been renumbered so that they appear in text in numerical order. Please verify that text citations refer to the correct renumbered references, throughout the Letter.

4 NOTE: External links, which appear as blue text in the reference section, are created for any reference where a Digital Object Identifier (DOI) can be found. Please confirm that the links created in this PDF proof, which can be checked by clicking on the blue text, direct the reader to the correct references online. If there is an error, correct the information in the reference or supply the correct DOI for the reference. If no correction can be made or the correct DOI cannot be supplied, the link will be removed.

5 Please provide author name for Ref. [2].

6 Please provide brief description to be included in Ref. [33]. The URL link will be activated at the time of publication.

Titles in References

The editors now encourage insertion of article titles in references to journal articles and e-prints. This format is optional, but if chosen, authors should provide titles for *all* eligible references. If article titles remain missing from eligible references, the production team will remove the existing titles at final proof stage.

ORCIDs

Please follow any ORCID links (iD) after the authors’ names and verify that they point to the appropriate record for each author.

Funding Information

Information about an article's funding sources is now submitted to Crossref to help you comply with current or future funding agency mandates. Crossref's Open Funder Registry (https://www.crossref.org/services/funder-registry/) is the definitive registry of funding agencies. Please ensure that your acknowledgments include all sources of funding for your article following any requirements of your funding sources. Where possible, please include grant and award ids. Please carefully check the following funder information we have already extracted from your article and ensure its accuracy and completeness:

- National Research Foundation of Korea, FundRef ID http://dx.doi.org/10.13039/501100003725 (Republic of Korea/KR)

Other Items to Check

- Please note that the original manuscript has been converted to XML prior to the creation of the PDF proof, as described above. Please carefully check all key elements of the paper, particularly the equations and tabular data.
- Title: Please check; be mindful that the title may have been changed during the peer-review process.
- Author list: Please make sure all authors are presented, in the appropriate order, and that all names are spelled correctly.
- Please make sure you have inserted a byline footnote containing the email address for the corresponding author, if desired. Please note that this is not inserted automatically by this journal.
- Affiliations: Please check to be sure the institution names are spelled correctly and attributed to the appropriate author(s).
- Receipt date: Please confirm accuracy.
- Acknowledgments: Please be sure to appropriately acknowledge all funding sources.
- References: Please check to ensure that titles are given as appropriate.
- Hyphenation: Please note hyphens may have been inserted in word pairs that function as adjectives when they occur before a noun, as in “x-ray diffraction,” “4-mm-long gas cell,” and “*R*-matrix theory.” However, hyphens are deleted from word pairs when they are not used as adjectives before nouns, as in “emission by x rays,” “was 4 mm in length,” and “the *R* matrix is tested.”
  Note also that Physical Review follows U.S. English guidelines in that hyphens are not used after prefixes or before suffixes: superresolution, quasiequilibrium, nanoprecipitates, resonancelike, clockwise.
- Please check that your figures are accurate and sized properly. Make sure all labeling is sufficiently legible. Figure quality in this proof is representative of the quality to be used in the online journal. To achieve manageable file size for online delivery, some compression and downsampling of figures may have occurred. Fine details may have become somewhat fuzzy, especially in color figures. The print journal uses files of higher resolution and therefore details may be sharper in print. Figures to be published in color online will appear in color on these proofs if viewed on a color monitor or printed on a color printer.
- Overall, please proofread the entire *formatted* article very carefully. The redlined PDF should be used as a guide to see changes that were made during copyediting. However, note that some changes to math and/or layout may not be indicated.

Ways to Respond

- ***Web:*** If you accessed this proof online, follow the instructions on the web page to submit corrections.
- ***Email:*** Send corrections to aps-robot@luminad.com. Include the accession code LG17581 in the subject line.
- ***Fax:*** Return this proof with corrections to +1.855.808.3897.

If You Need to Call Us

You may leave a voicemail message at +1.855.808.3897. Please reference the accession code and the first author of your article in your voicemail message. We will respond to you via email.

Resource-Efficient Topological Fault-Tolerant Quantum Computation with Hybrid Entanglement of Light

S. Omkar,* Yong Siah Teo, and Hyunseok Jeong†
Department of Physics and Astronomy, Seoul National University, 08826 Seoul, Republic of Korea

(Received 9 July 2019; accepted 1 July 2020)

We propose an all-linear-optical scheme to ballistically generate a cluster state for measurement-based topological fault-tolerant quantum computation using hybrid photonic qubits entangled in a continuous-discrete domain. Availability of near-deterministic Bell-state measurements on hybrid qubits is exploited for this purpose. In the presence of photon losses, we show that our scheme leads to a significant enhancement in both tolerable photon-loss rate and resource overheads. More specifically, we report a photon-loss threshold of $\sim 3.3\times 10^{-3}$, which is higher than those of known optical schemes under a reasonable error model. Furthermore, resource overheads to achieve logical error rate of $10^{-6}(10^{-15})$ is estimated to be $\sim 8.5\times 10^{5}(1.7\times 10^{7})$, which is significantly less by multiple orders of magnitude compared to other reported values in the literature.

DOI:

Errors during quantum information processing are unavoidable, and they are a major obstacle against practical implementations of quantum computation (QC) [1]. Quantum error correction (QEC) [2] permits scalable QC with faulty qubits and gates provided the noise is below a certain threshold. The noise threshold is determined by the details of the implementing scheme and the noise model.

Measurement-based topological fault-tolerant (FT) QC [3] on a cluster state provides a high error threshold of 0.75% against computational errors [4,5]. Additionally, it can tolerate qubit losses [6,7] and missing edges [8]; thus, it would be suitable for practical large-scale QC. However, there is a trade-off between the tolerable computational error rate, and the tolerable level of qubit losses and missing edges. A cluster state $|\mathcal{C}\rangle$, over a collection of qubits $\mathcal{C}$, is the state stabilized by operators $X_a \bigotimes_{b\in \mathrm{nh(a)}} Z_b$, where $a,b\in\mathcal{C}$, Z_i and X_i are the Pauli operators on the ith qubit, and nh(a) represents the adjacent neighborhood of qubit $a\in\mathcal{C}$ [9]. It has the form: $|\mathcal{C}\rangle=\prod_{b\in \mathrm{nh}(a)}\mathrm{CZ}_{a,b}|+\rangle_a|+\rangle_b$, $\forall\ a\in\mathcal{C}$, where CZ is the controlled-Z gate, $|\pm\rangle=(|0\rangle\pm|1\rangle)/\sqrt{2}$, and $\{|0\rangle,|1\rangle\}$ are eigenstates of Z. Here, we consider the Raussendorf cluster state $|\mathcal{C}_{\mathcal{L}}\rangle$ [3] on a cubic lattice $\mathcal{L}$ with qubits mounted on its faces and edges.

The linear optical platform has the advantage of quick gate operations compared to their decoherence time [10]. Unfortunately, schemes based on discrete variables (DV) like photon polarizations suffer from the drawback that the entangling operations (EOs), typically implemented by Bell-state measurements, are nondeterministic [11]. This leaves the edges corresponding to all failed EOs missing, and beyond a certain failure rate the cluster state cannot support QC. References [8,12–15] tackle this shortcoming with a repeat-until-success strategy. However, this strategy incurs heavy resource overheads in terms of both qubits and EO trials, and the overheads grow exponentially as the success rate of EO falls [8]. Moreover, conditioned on the outcome of the EO, all other redundant qubits must be removed *via* measurements [14] which would add to undesirable resource overheads. These schemes also require active switching to select successful outcomes of EOs and feed them to the next stage, which is known to have an adverse effect on the photon-loss threshold for FTQC [16]. DV-based optical EOs have a success rate of 50% that can be further boosted with additional resources like single photons [17], Bell states [18], and the squeezing operation [19]. Reference [20] uses EOs with a boosted success rate of 75% to build cluster states. This can be further enhanced by allotting more resources. Coherent-state qubits, composed of coherent states $|\pm\alpha\rangle$ of amplitudes $\pm\alpha$, enable one to perform nearly deterministic Bell-state measurements and universal QC using linear optics [21,22], while this approach is generally more vulnerable to losses [10,23]. Along this line, a scheme to generate cluster states for topological QC was suggested, but the value of α required to build a cluster state of sufficiently high fidelity is unrealistically large as $\alpha>20$ [24]. A hybrid qubit using both DV and continuous-variable (CV) states of light, i.e., polarized single photons and coherent states was introduced to take advantages of both the approaches [25].

We propose an all-linear-optical, measurement-based FT hybrid topological QC (HTQC) scheme on $|\mathcal{C}_{\mathcal{L}}\rangle$ of hybrid qubits. The logical basis for a hybrid qubit is defined as $\{|\alpha\rangle|H\rangle\equiv|0_L\rangle,|-\alpha\rangle|V\rangle\equiv|1_L\rangle\}$, where $|H\rangle$ and $|V\rangle$ are single-photon states with horizontal and vertical polarizations in the Z direction. The issues with indeterminism of EOs on DVs [8,13–15] and poor fidelity of the cluster states with CVs [24] are then overcome. Crucial to our scheme is a near-deterministic hybrid Bell-state measurement (HBSM) on hybrid qubits using two photon number parity detectors (PNPDs) and two on-off photodetectors (PDs), which is distinct from the previous version that requires two additional PDs to complete a teleportation protocol [25]. We only need HBSMs acting on three-hybrid-qubit cluster states to generate $|\mathcal{C}_{\mathcal{L}}\rangle$ without any active switching and feed forward. The outcomes of HBSMs are noted to interpret the measurement results during QEC and QC. In this sense, our scheme is *ballistic* in nature. Both CV and DV modes of hybrid qubits support the HBSMs to build $|\mathcal{C}_{\mathcal{L}}\rangle$, while only DV modes suffice for QEC and QC. This means that *only* on-off PDs for DV modes are required once $|\mathcal{C}_{\mathcal{L}}\rangle$ is generated. In addition, photon loss is ubiquitous [10], which causes dephasing such as in [23,25,26]. We analyze the performance of our scheme against photon losses and compare it with the known all-optical schemes.

Physical platform for $|\mathcal{C}_{\mathcal{L}}\rangle$.—To ballistically build a $|\mathcal{C}_{\mathcal{L}}\rangle$, we begin with hybrid qubits, in the form $(|H\rangle|\alpha\rangle + |\mathrm{v}\rangle|-\alpha\rangle)/\sqrt{2} = (|0_L\rangle + |1_L\rangle)/\sqrt{2} \equiv |+_L\rangle$, as raw resources of our scheme. In fact, this type of hybrid qubits and with slight variant forms (with the vacuum and single photon instead of $|H\rangle$ and $|V\rangle$) were generated in recent experiments [27–29], which can also be used for QC in the same way as in [25] even with higher fidelities and success probabilities of teleportation [30]. A hybrid qubit can also be generated using a Bell-type photon pair, a coherent-state superposition, linear optical elements and four PDs [31].

The HBSM introduced in this Letter consists of two types of measurements, B_α and B_s, acting on CV and DV modes, respectively. A Bell-state measurement for coherent-state qubits [32], B_α, comprises of a beam splitter (BS) and two PNPDs, whereas B_s has a polarizing BS (PBS) and two PDs as shown in Fig. 1(a). The failure rate for an HBSM turns out to be $p_f = e^{-2\alpha^2}/2$ (see the Supplemental Material [33] and also [25]) that rapidly approaches zero with growing α. The first and only nondeterministic step of our protocol is to prepare two kinds of three-hybrid-qubit cluster states,

$$
\begin{aligned}
|\mathcal{C}_3\rangle_{abc} &= \frac{1}{2}(|0_L\rangle_a|0_L\rangle_b|0_L\rangle_c + |0_L\rangle_a|0_L\rangle_b|1_L\rangle_c \\
&\quad + |1_L\rangle_a|1_L\rangle_b|0_L\rangle_c - |1_L\rangle_a|1_L\rangle_b|1_L\rangle_c), \\
|\mathcal{C}_{3'}\rangle_{abc} &= \frac{1}{\sqrt{2}}(|0_L\rangle_a|0_L\rangle_b|0_L\rangle_c + |1_L\rangle_a|1_L\rangle_b|1_L\rangle_c), \qquad (1)
\end{aligned}
$$

using four hybrid qubits, two B_αs and a B_{I} [33]. (Here, B_{I} is a type-I fusion gate using two PBSs, two PDs and a $\pi/2$ rotator, of which the success probability is $1/2$. See the

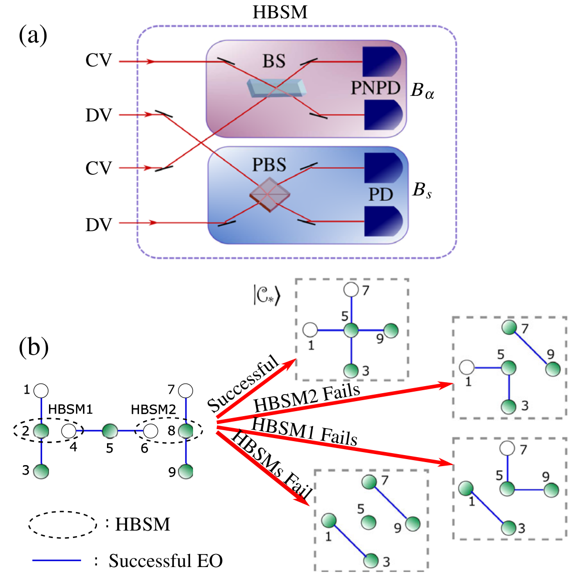

FIG. 1. (a) B_α acts on CV modes and fails when neither of the two PNPDs click. The failure rate of a B_α on the hybrid qubits is $e^{-2\alpha^2}$. $\mathrm{B_s}$ acts on DV modes and is successful with probability $1/2$ only when both the PDs click. (b) The three-hybrid-qubit cluster with one unfilled circle represents $|\mathcal{C}_3\rangle$, while that with two represents $|\mathcal{C}_{3'}\rangle$ in Eq. (1). An unfilled circle means a difference by a Hadamard transform from the original three-qubit cluster (see the Supplemental Material [33]). Success of both HBSMs creates a star cluster $|\mathcal{C}_*\rangle$ and other cases lead to distorted star clusters as shown.

Supplemental Material for details [33].) As shown in Fig. 1(b), an HBSM is performed on modes 2 and 4 of $|\mathcal{C}_3\rangle_{123}$ and $|\mathcal{C}_{3'}\rangle_{456}$, and the other HBSM is performed similarly between $|\mathcal{C}_{3'}\rangle_{456}$ and $|\mathcal{C}_3\rangle_{789}$, which produces a star cluster, $|\mathcal{C}_*\rangle$, with a high success probability. Simultaneously, the star clusters are connected using HBSMs to form layers of $|\mathcal{C}_{\mathcal{L}}\rangle$ as depicted in Fig. 2(b). As the third dimension of $|\mathcal{C}_{\mathcal{L}}\rangle$ is time simulated, in practice only two physical layers suffice for QC [4].

Notably, different outcomes of HBSMs and failures during this process can be compensated during QEC as explained below. As HBSMs have four possible outcomes from B_α, the built cluster state is equivalent to $|\mathcal{C}_{\mathcal{L}}\rangle$ up to local Pauli operations. This can be compensated by accordingly making bit flips to the measurement outcomes during QEC. This is achieved by classical processing and no additional quantum resources are required. As shown in Fig. 1(b), failure(s) of HBSMs result(s) in a *deformed* star cluster with diagonal edge(s) instead of four proper edges stretching from the central qubit. The final cluster state $|\mathcal{C}_{\mathcal{L}}\rangle$ inherits these diagonal edges as shown in Fig. 2(c) with a *disturbed* stabilizer structure. However, failures of HBSMs are heralded, which reveals the locations of such diagonal edges. These diagonal edges can be removed by adaptively measuring the hybrid qubits in a Z basis (M_Z), as shown in Fig. 2(c), restoring back the

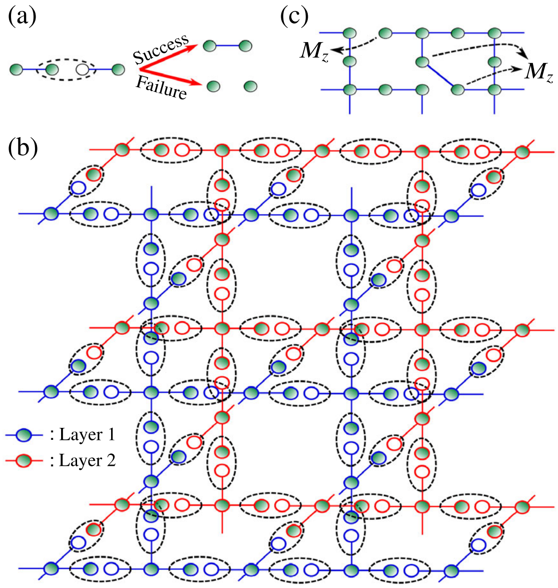

FIG. 2. (a) When connecting $|\mathcal{C}_*\rangle$ s, a successful HBSM creates an edge between hybrid qubits whereas a failed HBSM leaves the edge missing. (b) 3D illustration of building two layers of $|\mathcal{C}_\mathcal{L}\rangle$ for practical HTQC with $|\mathcal{C}_*\rangle$s and HBSMs to connect them. (c) A diagonal edge is created due to failure of an HBSM corresponding to $|\mathcal{C}_*\rangle$, and a missing edge is due to failure of an HBSM while connecting them. A single layer of $|\mathcal{C}_\mathcal{L}\rangle$ is shown for convenience, and M_z is measurement on a Z basis.

stabilizer structure of $|\mathcal{C}_\mathcal{L}\rangle$. Failure of HBSMs for connecting $|\mathcal{C}_*\rangle$s simply leaves the edges missing, as shown in Fig. 2(a), without distorting the stabilizer structure.

Noise model.—Let η be the photon-loss rate due to imperfect sources and detectors, absorptive optical components and storages. In HTQC, the effect of photon loss is threefold (see the Supplemental Material [33] and also [25]) that (i) causes dephasing of hybrid qubits, i.e., phase-flip errors Z, a form of computational error, with rate $p_Z = [1-(1-\eta)e^{-2\eta\alpha^2}]/2$, (ii) lowers the success rate of HBSM, and (iii) makes hybrid qubits leak out of the logical basis. Quantitatively, p_f increases to $(1+\eta)e^{-2\alpha'^2}/2$, where $\alpha' = \sqrt{1-\eta}\alpha$. Thus, for a given η and growing α we face a trade-off between the desirable success rate of HBSM and the detrimental dephasing rate p_Z.

Further, like the type-II fusion gate in [34], B_s does not introduce computational errors during photon loss [33]. However, the action of B_α on the lossy hybrid qubits introduces additional dephasing as shown in the Supplemental Material [33]. To clarify, like DV schemes [15], photon loss does not imply hybrid-qubit loss. In many FTQC schemes η has a typical operational value of $\sim 10^{-3}$ (on the higher side) [13,26,35,36], i.e., $\eta \ll 1$. The probability of hybrid-qubit loss due to photon loss, $\eta e^{-\alpha'^2}$ (the overlap between a lossy hybrid qubit and the vacuum), is then very small compared to p_f and negligible to HTQC.

Measurement-based HTQC.—Once the faulty cluster state is built with missing and diagonal edges, and phase-flip errors on the constituent hybrid qubits, measurement-based HTQC is performed by making sequential single-qubit measurements in X and Z bases. A few chosen ones are measured on a Z basis to create defects, and the rest are measured on a X basis for error syndromes during QEC and for effecting the Clifford gates on the logical states of $|\mathcal{C}_\mathcal{L}\rangle$. For magic state distillation, measurements are made on a $(X \pm Y)/\sqrt{2}$ basis [3–5]. All these measurements are accomplished by measuring only polarizations of DV modes in their respective bases. These measurement outcomes should be interpreted with respect to the recorded HBSM outcomes as mentioned earlier.

Simulations.—Simulations of topological QEC are performed using AUTOTUNE [37] (see Sec. IV of the Supplemental Material [33]). Only the central hybrid qubit of $|\mathcal{C}_*\rangle$ remains in the cluster and the rest are utilized by HBSMs. The $|\mathcal{C}_*\rangle$'s are arranged as shown in Fig. 2. Next, all hybrid qubits are subjected to dephasing of rate p_Z following which EOs are performed using HBSMs. The action of B_α in HBSM dephases the adjacent remaining hybrid qubits, which can be modeled as applying $\{Z \otimes I, I \otimes Z\}$ with rate p_Z. Section III of the Supplemental Material [33] presents technical details. This concludes the simulation of building noisy $|\mathcal{C}_\mathcal{L}\rangle$. Further, the hybrid qubits waiting to undergo measurements as a part of QEC attract dephasing, and rate p_Z again is assigned. During QEC, X-measurement outcomes used for syndrome extraction could be erroneous. This error too is assigned rate p_Z. Due to photon losses, the hybrid qubits leak out of the logical basis failing the measurements on DV modes. This leakage is also assigned p_Z, which only overestimates η.

One missing edge due to failed HBSMs can be mapped to two missing hybrid qubits [8]. Improving on this, by adaptively performing M_Z [Fig. 2(c)] on one of the hybrid qubits associated with a missing edge, this edge can be modeled with a missing qubit [38]. Then, QEC is carried out as in the case of missing qubits [6]. In constructing $|\mathcal{C}_\mathcal{L}\rangle$, an equal number of HBSMs are required for building $|\mathcal{C}_*\rangle$ and for connecting them. A failure of an HBSM during the former process corresponds to two hybrid-qubit losses, and the latter case to one [Fig. 2(c)]. Therefore, on average 1.5 hybrid qubits per HBSM failure are lost. Percolation threshold for $|\mathcal{C}_\mathcal{L}\rangle$ is a 0.249 fraction of missing qubits [6,39,40], which corresponds to $\alpha \approx 0.7425$ (when no computational error is tolerated, i.e., $\eta = 0$), the critical value of α below which HTQC becomes impossible.

Results.—The logical error rate p_L (failure rate of topological QEC [4]) was determined against various values of p_Z for $|\mathcal{C}_\mathcal{L}\rangle$ of code distances $d = 3$, 5, 7. This was repeated for various values of p_f, which correspond to different values of α. Figure 3(a) shows the simulation results for $\alpha_{\rm opt} = 1.247$ in which the intersection point of the curves corresponds to the threshold dephasing rate

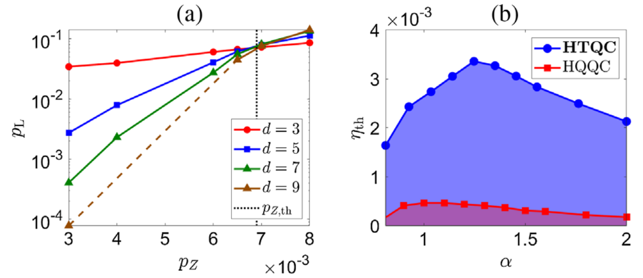

FIG. 3. (a) Logical error rate p_L is plotted against the dephasing rate p_Z for coherent-state amplitude $\alpha_{\text{opt}} = 1.247$ and code distances $d = 3$, 5, 7. The intersecting point of these curves corresponds to the threshold dephasing rate $p_{Z,\text{th}}$. (b) The tolerable photon-loss rate η_{th} is plotted against coherent-state amplitude α. The behavior of the curve is due to the trade-off between the success rate of HBSM and dephasing rate p_Z with growing α. As we increase α, both the success rate and p_Z increase; but the former dominates and leads to an increase in η_{th}. When $\alpha > 1.247$, p_Z dominates and causes η_{th} to decrease. Compared to the nontopological HQQC [25], HTQC has an order of higher value for η_{th}.

$p_{Z,\text{th}}$. The photon-loss threshold η_{th} is determined using the expression for p_Z.

Figure 3(b) shows the behavior of η_{th} with α. Owing to the trade-off between p_f and p_Z, the optimal value for HTQC is $\alpha_{\text{opt}} \approx 1.25$ which corresponds to $\eta_{\text{th}} \approx 3.3 \times 10^{-3}$ and $p_{Z,\text{th}} \approx 6.9 \times 10^{-3}$. The value of η_{th} for $0.8 \le \alpha \le 2$ is on the order of 10^{-3}, which is an order greater than the non-topological hybrid-qubit-based QC (HQQC) [25] and coherent state QC (CSQC) [23]. HTQC also outperforms the DV based topological photonic QC (TPQC) with $\eta_{\text{th}} \approx 5.5 \times 10^{-4}$ [15]. Multiphoton qubit QC (MQQC) [26], parity state linear optical QC (PLOQC) [35] and error-detecting, quantum state transfer based QC (EDQC) [36] provide η_{th}s, which are less than HTQC but of the same order as illustrated in Fig. 4(a). In addition, η and the computational error rates are independent in [13,35,36], while these two quantities are related in our scheme and Refs. [23,25,26]. Also in the former schemes the computational error is dephasing in nature, and in the latter schemes it is depolarizing. In fact, η_{th}s claimed by optical cluster-state QC (OCQC) [13], PLOQC, EDQC, and TPQC are valid only for zero computational error. This is unrealistic because photon losses typically cause computational errors. For the computational error rate as low as 8×10^{-5}, $\eta_{\text{th}} = 0$ in OCQC. Thus, for *nonzero* computational errors, HTQC also outperforms OCQC due to its topological nature of QEC.

To estimate the resource overhead per gate operation, we count the average number of hybrid qubits N required to build $|\mathcal{C}_{\mathcal{L}}\rangle$ of a sufficiently large side length l, where the desired value of l depends on the target p_L. The length l is determined such that $|\mathcal{C}_{\mathcal{L}}\rangle$ can accommodate defects of circumference d which are separated by distance d [7]. For this, the length of sides must be at least $l = 5d/4$. Extrapolating the suppression of p_L with code distance, we determine the value of d required to achieve the target p_L using the expression $p_L = a'/[(a/a')^{(d-d_{a'})/2}]$ [7], where a and a' are values of p_L corresponding to the second highest and the highest distances, d_a and $d_{a'}$, chosen for simulation. Once d is determined, N can be estimated as follows. Recall that two $|\mathcal{C}_3\rangle$s and a $|\mathcal{C}_{3'}\rangle$ are needed to build a $|\mathcal{C}_*\rangle$. On average, $8/[(1-e^{-2\alpha^2})^2]$ hybrid qubits are needed to create a three-hybrid-qubit cluster (see Sec. III of the Supplemental Material [33]) and a total of $24/[(1-e^{-2\alpha^2})^2]$ hybrid qubits for a $|\mathcal{C}_*\rangle$. Each $|\mathcal{C}_*\rangle$ corresponds to a single hybird qubit in the $|\mathcal{C}_{\mathcal{L}}\rangle$ and thus the number of $|\mathcal{C}_*\rangle$s needed is $6l^3$. Finally, on average, $1125d^3/[4(1-e^{-2\alpha^2})^2]$ hybrid qubits are incurred. For the optimal value of $\alpha_{\text{opt}} \approx 1.25$, from Fig. 3(a) we have $a \approx 4.4 \times 10^{-4}$, $a' \approx 7.9 \times 10^{-5}$, and $d_{a'} = 9$; using these in the expression for p_L we find that $d \approx 14(38)$ is needed to achieve $p_L \sim 10^{-6}(10^{-15})$. This incurs $N \approx 8.5 \times 10^5 (1.7 \times 10^7)$ hybrid qubits.

Comparisons in Fig. 4(b) and in the Supplemental Material [33] show that HTQC incurs resources significantly less than all the other schemes under consideration. As an example, for the case of TPQC, we find that $a = 0.065$ and $a' = 0.059$ from Fig. 7(a) of [15], where the figure considers only computational errors. Thus, TPQC under computational errors needs $d = 225(621)$ to attain $p_L \sim 10^{-6}(10^{-15})$. Since a qubit in TPQC needs $2R+1$ photons on average as resources [15], we obtain $N = (2R+1) \times 6(5d/4)^3$ [33], where $R = 7$ for maximum η_{th} [15]. We then find $N = 2 \times 10^9$ (4.2×10^{10}) for TPQC,

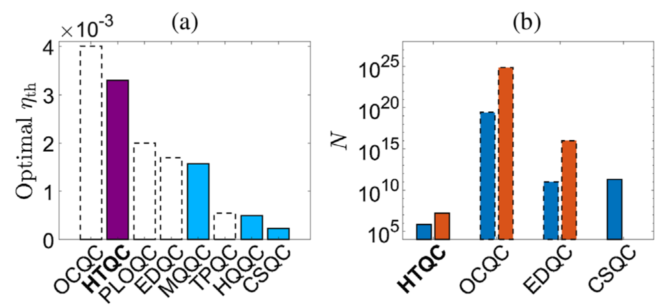

FIG. 4. (a) Optimal photon-loss threshold η_{th} for various QC schemes. It should be noted that η_{th}s of OCQC, PLOQC, EDQC, and TPQC (dashed borders) are valid only for zero computational error, which is physically unachievable. Other schemes evaluate optimal η_{th} at nonzero computational errors naturally related to η. (b) Resource overhead N to achieve logical error rate $p_L \sim 10^{-6}$(blue shorter bars) and $p_L \sim 10^{-15}$(orange taller bars) in terms of the average numbers of hybrid qubits (HTQC), entangled photon pairs (OCQC and EDQC), coherent-state superpositions (CSQC) from our analysis and published data in [13,23,36]. For CSQC data only for $p_L \sim 10^{-6}$ is available [23]. Obviously, HTQC is practically favorable for large scale QC both in terms of η_{th} and N. See the Supplemental Material [33] for more details of comparisons.

and it must be even larger when qubit losses are considered together with computational errors [33].

Discussion.—Our proposal permits the construction of cluster states with very few missing edges that subsequently support QEC and QC only with photon on-off measurements. We simulated its performance and found that our scheme is significantly more efficient than other known schemes in terms of both resource overheads and photon-loss thresholds (Fig. 4), especially when exceedingly small logical error rates are desired for large-scale QC. We have considered measurements only on DV modes of hybrid qubits for QEC. However, measurements on CV modes can also be used, which will significantly reduce leakage errors and improve the photon-loss threshold. The scheme requires hybrid qubits of $\alpha \approx \sqrt{2} \times 1.25$ as raw resource states, which can in principle be generated using available optical sources, linear optics, and photodetectors [28,29,31].

One may examine other decoders tailored to take advantage of dephasing noise, such as in [41] instead of the minimum weight perfect match [42], for improvement of the photon-loss threshold. Different single-qubit noise models [43] may be considered to study the performance of HTQC. A sideline task would be *in situ* noise characterization using the available syndrome data [44–47]. The procedure proposed here to build complex hybrid clusters can also be used to build lattices of other geometries for QC [20,48,49] and other tasks such as communication [50].

We thank A. G. Fowler for useful discussions and S.-W. Lee for providing data from [25] used in Fig. 3. This work was supported by National Research Foundation of Korea (NRF) grants funded by the Korea government (Grants No. 2019M3E4A1080074 and No. 2020R1A2C1008609). Y. S. T. was supported by an NRF grant funded by the Korea government (Grant No. NRF-2019R1A6A1A10073437).

[*]omkar.shrm@gmail.com
[†]h.jeong37@gmail.com

[1] M. A. Nielsen and I. L. Chuang, *Quantum Computation and Quantum Information* (Cambridge University Press, Cambridge, England, 2010).
[2] *Quantum Error Correction* (Cambridge University Press, Cambridge, England, 2013).
[3] R. Raussendorf, J. Harrington, and K. Goyal, Ann. Phys. (Amsterdam) **321**, 2242 (2006).
[4] R. Raussendorf, J. Harrington, and K. Goyal, New J. Phys. **9**, 199 (2007).
[5] R. Raussendorf and J. Harrington, Phys. Rev. Lett. **98**, 190504 (2007).
[6] S. D. Barrett and T. M. Stace, Phys. Rev. Lett. **105**, 200502 (2010).
[7] A. C. Whiteside and A. G. Fowler, Phys. Rev. A **90**, 052316 (2014).
[8] Y. Li, S. D. Barrett, T. M. Stace, and S. C. Benjamin, Phys. Rev. Lett. **105**, 250502 (2010).
[9] H. J. Briegel and R. Raussendorf, Phys. Rev. Lett. **86**, 910 (2001).
[10] T. C. Ralph and G. J. Pryde, Prog. Opt. **54**, 209 (2010).
[11] D. E. Browne and T. Rudolph, Phys. Rev. Lett. **95**, 010501 (2005).
[12] M. A. Nielsen, Phys. Rev. Lett. **93**, 040503 (2004).
[13] C. M. Dawson, H. L. Haselgrove, and M. A. Nielsen, Phys. Rev. A **73**, 052306 (2006).
[14] K. Fujii and Y. Tokunaga, Phys. Rev. Lett. **105**, 250503 (2010).
[15] D. A. Herrera-Martí, A. G. Fowler, D. Jennings, and T. Rudolph, Phys. Rev. A **82**, 032332 (2010).
[16] Y. Li, P. C. Humphreys, G. J. Mendoza, and S. C. Benjamin, Phys. Rev. X **5**, 041007 (2015).
[17] F. Ewert and P. van Loock, Phys. Rev. Lett. **113**, 140403 (2014).
[18] W. P. Grice, Phys. Rev. A **84**, 042331 (2011).
[19] H. A. Zaidi and P. van Loock, Phys. Rev. Lett. **110**, 260501 (2013).
[20] M. Gimeno-Segovia, P. Shadbolt, D. E. Browne, and T. Rudolph, Phys. Rev. Lett. **115**, 020502 (2015).
[21] H. Jeong and M. S. Kim, Phys. Rev. A **65**, 042305 (2002).
[22] T. C. Ralph, A. Gilchrist, G. J. Milburn, W. J. Munro, and S. Glancy, Phys. Rev. A **68**, 042319 (2003).
[23] A. P. Lund, T. C. Ralph, and H. L. Haselgrove, Phys. Rev. Lett. **100**, 030503 (2008).
[24] C. R. Myers and T. C. Ralph, New J. Phys. **13**, 115015 (2011).
[25] S.-W. Lee and H. Jeong, Phys. Rev. A **87**, 022326 (2013).
[26] S.-W. Lee, K. Park, T. C. Ralph, and H. Jeong, Phys. Rev. Lett. **114**, 113603 (2015).
[27] D. V. Sychev, A. E. Ulanov, E. S. Tiunov, A. A. Pushkina, A. Kuzhamuratov, V. Novikov, and A. I. Lvovsky, Nat. Commun. **9**, 3672 (2018).
[28] H. Jeong, A. Zavatta, M. Kang, S.-W. Lee, L. S. Costanzo, S. Grandi, T. C. Ralph, and M. Bellini, Nat. Photonics **8**, 564 (2014).
[29] O. Morin, K. Huang, J. Liu, H. Le Jeannic, C. Fabre, and J. Laurat, Nat. Photonics **8**, 570 (2014).
[30] H. Kim, S.-W. Lee, and H. Jeong, Quantum Inf. Process. **15**, 4729 (2016).
[31] H. Kwon and H. Jeong, Phys. Rev. A **91**, 012340 (2015).
[32] H. Jeong, M. S. Kim, and J. Lee, Phys. Rev. A **64**, 052308 (2001).
[33] See the Supplemental Material at http://link.aps.org/supplemental/10.1103/PhysRevLett.000.000000 for [brief description].
[34] M. Varnava, D. E. Browne, and T. Rudolph, Phys. Rev. Lett. **100**, 060502 (2008).
[35] A. J. F. Hayes, H. L. Haselgrove, A. Gilchrist, and T. C. Ralph, Phys. Rev. A **82**, 022323 (2010).
[36] J. Cho, Phys. Rev. A **76**, 042311 (2007).
[37] A. G. Fowler, A. C. Whiteside, A. L. McInnes, and A. Rabbani, Phys. Rev. X **2**, 041003 (2012).
[38] J. M. Auger, H. Anwar, M. Gimeno-Segovia, T. M. Stace, and D. E. Browne, Phys. Rev. A **97**, 030301(R) (2018).
[39] C. D. Lorenz and R. M. Ziff, Phys. Rev. E **57**, 230 (1998).

[40] M. Pant, D. Towsley, D. Englund, and S. Guha, Nat. Commun. **10**, 1070 (2019).
[41] D. K. Tuckett, S. D. Bartlett, and S. T. Flammia, Phys. Rev. Lett. **120**, 050505 (2018).
[42] A. G. Fowler, Phys. Rev. Lett. **109**, 180502 (2012).
[43] S. Omkar, R. Srikanth, and S. Banerjee, Quantum Inf. Process. **12**, 3725 (2013).
[44] S. Omkar, R. Srikanth, and S. Banerjee, Phys. Rev. A **91**, 012324 (2015).
[45] S. Omkar, R. Srikanth, and S. Banerjee, Phys. Rev. A **91**, 052309 (2015).
[46] S. Omkar, R. Srikanth, S. Banerjee, and A. Shaji, Ann. Phys. (Amsterdam) **373**, 145 (2016).
[47] A. G. Fowler, D. Sank, J. Kelly, R. Barends, and J. M. Martinis, arXiv:quant-ph/1405.1454.
[48] H. Bombin and M. A. Martin-Delgado, Phys. Rev. Lett. **98**, 160502 (2007).
[49] H. A. Zaidi, C. Dawson, P. van Loock, and T. Rudolph, Phys. Rev. A **91**, 042301 (2015).
[50] K. Azuma, K. Tamaki, and H.-K. Lo, Nat. Commun. **6**, 6787 (2015).